PERGAMON

Chemical Engineering Science 54 (1999) 3521–3531

Chemical Engineering Science

Growth, microstructure, and permeation properties of supported zeolite (MFI) films and membranes prepared by secondary growth

George Xomeritakis[a], Anastasios Gouzinis[a], Sankar Nair[a], Tatsuya Okubo[b], Mingyan He[c], Rene M. Overney[c], Michael Tsapatsis[a,*]

[a]*Department of Chemical Engineering, University of Massachusetts, Amherst, MA 01003, USA*
[b]*Department of Chemical System Engineering, The University of Tokyo, 7-3-1 Hongo, Bonkyo-ku, Tokyo 113, Japan*
[c]*Department of Chemical Engineering, University of Washington, Box 351750, Seattle, WA 98195-1750, USA*

Abstract

MFI polycrystalline films were prepared on non-porous glass as well as on porous alumina substrates, using secondary growth of seed layers. The secondary growth procedure consists of deposition of MFI microcrystals from a colloidal suspension on the substrate to form seed layers, followed by hydrothermal growth of the seed crystals to form a film. *In situ* growth was also employed on non-porous substrates that were seed free. The two different growth procedures were compared and it was found that the presence of the seed layers affects film growth and final microstructure. The films upon secondary growth exhibit columnar grain microstructure. Depending on the secondary growth conditions the grains of the polycrystalline films may exhibit *c*- or [*h*0*h*]-out-of-plane orientation. We report single-component and binary permeation measurements using N_2, SF_6 and butane isomers, for MFI membranes prepared by secondary growth on porous alumina substrates. The $N_2:SF_6$ single-component selectivity is 8–10, while the permeation flux of n-C_4H_{10} and the n-C_4H_{10}:i-C_4H_{10} flux ratio from 50/50 mixtures at 22°C is in the range $1.5–5.5\times10^{-3}$ mol $m^{-2}s^{-1}$ and 28–62, respectively. The n-C_4H_{10}:i-C_4H_{10} flux ratio remains high up to 150°C but decreases drastically at higher temperatures. © 1999 Elsevier Science Ltd. All rights reserved.

Keywords: Zeolite membrane; Inorganic membrane; Silicalite-1; Seeded growth; Gas permeation

1. Introduction

The preparation of zeolite films with controlled microstructure, i.e. grain and grain boundary structure, grain orientation, thickness, and composition is desirable for a number of applications most notably as supported zeolite membranes for separations and catalytic applications (Bein, 1996; Brinker, 1998). MFI molecular sieve membranes that exhibit preferred orientation have been reported recently (Lai et al., 1996; Lovallo and Tsapatsis, 1996; Lovallo et al., 1998). These membranes were obtained by *secondary growth* of calcined MFI or MFI/alumina precursor layers. The secondary growth technique has been also employed for the preparation of zeolite A films (Boudreau and Tsapatsis, 1997; Boudreau et al., 1998) and randomly oriented films of zeolite L (Lovallo et al., 1996). Recently, Gouzinis and Tsapatsis (1998) applied the secondary growth technique on uncalcined/additive-free MFI precursor layers and demonstrated that the seed particles remain on the support surface and can grow to form highly oriented MFI films with columnar microstructure. It was also shown that under appropriate secondary growth conditions, the film growth can be manipulated leading to variations in the out-of-plane orientation.

In what follows, we report on the role of the uncalcined/additive free precursor layers and the secondary growth conditions on the formation, resulting microstructure and permeation properties of MFI films. In Section 3.1, the films obtained upon secondary growth are compared with films obtained by *in situ* growth on

*Corresponding author. Tel. 001 413 545 0276; fax: 001 413 545 1647; e-mail: tsapatsi@ecs.umass.edu.

0009-2509/99/$ – see front matter © 1999 Elsevier Science Ltd. All rights reserved.
PII: S0009-2509(98)00515-6

seed-free substrates. It is shown that the presence of seeds can dramatically affect the morphology of the resulting film even under secondary growth conditions that, in the absence of seed layers, can lead to nucleation and crystal growth in solution and on the substrate. Based on the current knowledge on the mechanism of MFI formation, we propose an explanation for the role of the seeds in film growth. Moreover, a characteristic defect that is occasionally observed after secondary growth is described, and its formation is attributed to gaps of the precursor layers. In Section 3.2, the ability to manipulate the orientation of the MFI films by the secondary growth conditions is summarized and the resulting surface morphologies are further investigated with surface force microscopy (SFM). In Section 3.3, we report permeances of butane isomers through alumina supported MFI membranes prepared by secondary growth and compare these with reported permeances of butane isomers through MFI membranes prepared by *in situ* growth.

2. Experimental

2.1. Synthesis

A colloidal suspension of discrete MFI (silicalite-1) particles (20 g/l, 100 nm diameter) was prepared as previously reported (Lovallo and Tsapatsis, 1996). The suspension was used for coating non-porous glass or porous alumina substrates with seed layers, but excluding the use of additives (e.g. alumina binder). The silicalite-coated substrates were dried in air at room temperature overnight and were placed vertically in Teflon lined autoclaves for hydrothermal treatment (*secondary growth*), using a solution with typical molar composition of $0.9TPAOH:950H_2O:16EtOH$. For *in situ* growth of MFI films, the same composition and glass substrates that were not coated with seed layers were used. The supports used for zeolite membrane preparation were home-made α-Al_2O_3 disks, 2 mm thick, 22 mm in diameter and 0.15 μm pore size. Only one side was coated with seeds. Secondary growth for the membranes reported was performed at 175°C, using a solution with composition $0.9\ MOH:0.9\ TPABr:4\ SiO_2:1000\ H_2O:16\ EtOH$, where M = Na or K. The substrates were placed in 35 ml Teflon-lined autoclaves.

2.2. Microstructural characterization

Scanning Electron Microscopy (SEM) was performed on a JEOL 100CX microscope operating in SEM mode at 20 kV. Higher resolution micrographs were recorded using a Hitachi S-900 FE-SEM. Phase identification and determination of any preferred orientation was performed by X-ray Diffraction (XRD) on a Phillips X'Pert system using Cu K_α radiation. Crystal planes that are parallel to the substrate are detected when the system is operated on a theta/2-theta geometry. XRD pole figure analysis was used to quantitate the degree of out-of-plane orientation. For these measurements, the two-theta reflection corresponding to a specific crystal plane was identified from the XRD pattern and the incidence and exit angle were fixed to this position. The sample was tilted from 0 to 85° (psi) and rotated 360° (phi) for each tilt angle. Film topology and crystal faces of singular crystal grains have been studied by a bi-directional scanning force microscope (SFM) from Topometrix Inc. (Explorer) with laser beam deflection detection scheme and silicon nitride cantilevers of 0.03 N/m at ambient conditions. The film surfaces have been scanned with 1 Hz per scan line in the x,y-plane which is provided by the glass substrate. The bi-directional SFM measures lateral forces simultaneously with normal forces (topography) acting on the probing tip, both over a localized contact area between probing tip and sample of a few square nanometers. Lateral force SFM mapping has been used to enhance the contrast of differently oriented crystal faces.

2.3. Permeation measurements

For permeation experiments the membranes were sealed with the aid of silicon rubber O-rings inside a custom made stainless steel permeation cell fixed inside a box furnace. A 50/50 *n*-butane/*i*-butane mixture was introduced into the permeator (the zeolite layer facing the gas feed) while the opposite side was flushed with a He stream. Mixture permeation data for butane isomers were obtained by analyzing the He sweep composition with the aid of a HP 5890 Series II Gas Chromatograph equipped with a 1/8″ SS packed column (0.19 picric acid on Graphpac, Alltech) and FID. Single gas permeation measurements were performed using a vacuum system with a calibrated receiving cylinder. Fig. 1 is a schematic of the permeation setup.

3. Results and discussion

3.1. Secondary versus in situ growth

The final film microstructure and its evolution are greatly affected by the presence of the seeds that are deposited on the substrate prior to secondary growth. This is clearly demonstrated in Fig. 2, which shows two MFI films that were prepared using secondary and *in situ* growth, and exhibit different microstructures. At early stages of secondary growth (after ~4 h), an intergrown

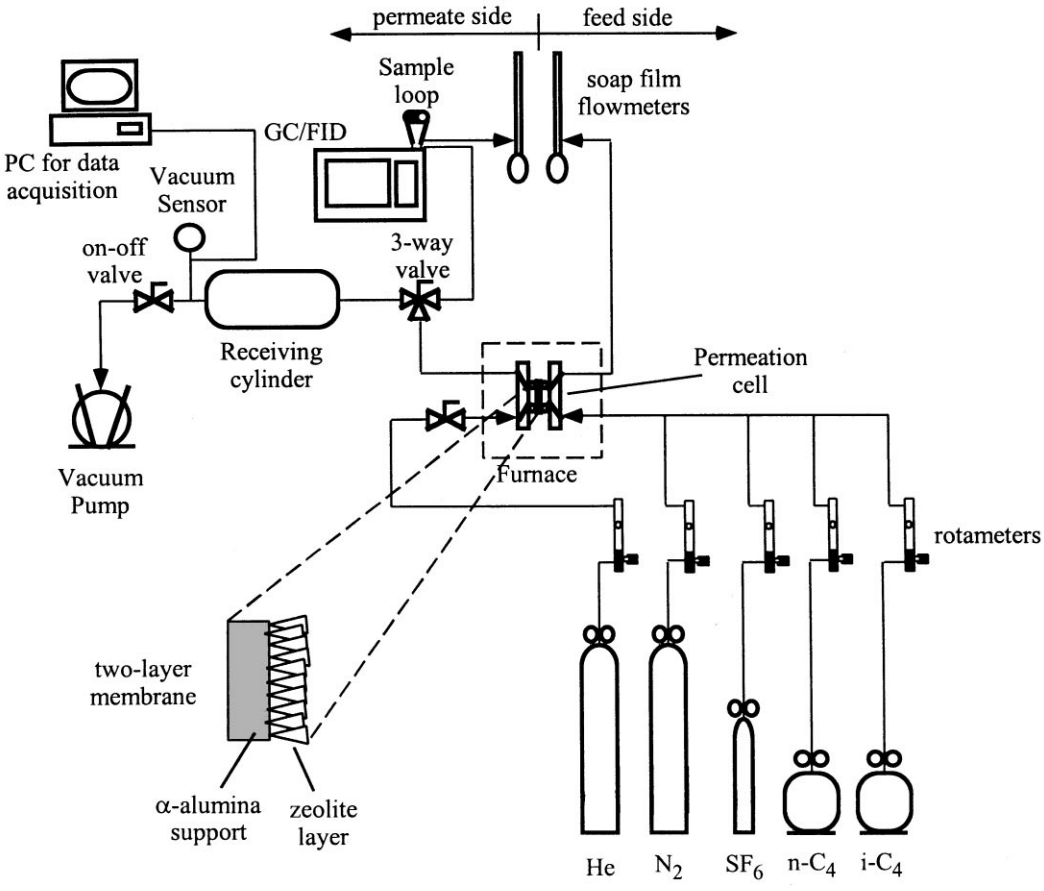

Fig. 1. Schematic representation of the experimental apparatus used for permeation measurements.

film was already formed on the seed-coated substrate as observed by FE-SEM (Fig. 2a). On the other hand, small crystals with a cubic morphology, well-developed facets and size of $\sim$20 nm were attached or nucleated on the non-seeded substrate during *in situ* hydrothermal treatment (Fig. 2c). The surface coverage of the seed-free substrate was very low at this stage and the presence of an amorphous gel surrounding the zeolite particles is evident from Fig. 2c. Such a gel formation was also observed in the report of Koegler et al. (1997) during *in situ* growth of MFI films on silicon wafers. Gel formation was not observed when seeds were present as shown in Fig. 2a. Further growth results, finally, in the microstructures presented in Figs. 2b and d after about 20 h. As can be seen from Fig. 2b in the case of the seed-coated substrate and for the specific growth conditions, an intergrown polycrystalline film with columnar grains and small surface roughness was formed. In the other case (uncoated substrate), as shown in Fig. 2d, large non-intergrown crystals cover the substrate. In agreement with other reports (Koegler et al., 1997), the XRD analysis (Fig. 2e, top) shows that the film obtained by *in situ* growth exhibits [0*k*0] or [*h*00]-out-of-plane preferred orientation. In contrast, the film obtained by secondary growth shows [*h*0*h*]-out-of-plane preferred orientation (Fig. 2e, bottom). The issue of the preferred orientation is further discussed in Section 3.2 and in what follows we address the reason for the dramatic influence of the precursor layer on film growth kinetics.

The possible events taking place in solution (Burkett and Burkett and Davis, 1995a, Dokter et al., 1995) and on a substrate (pure or seed-coated) during hydrothermal treatment are summarized schematically in Fig. 3. In the presence of the precursor layer the nucleation stage is bypassed and growth of the seed particles starts directly as soon as they come in contact with the secondary growth solution (Gouzinis and Tsapatsis, 1998). The results shown above clearly indicate that growth of the existing crystals, once initiated, is self-preserved by preventing the nucleation or incorporation of new crystals in the vicinity of the growing film. The steady consumption of nutrients, precursors and extended structures able to contribute to crystal growth is proposed as a possible

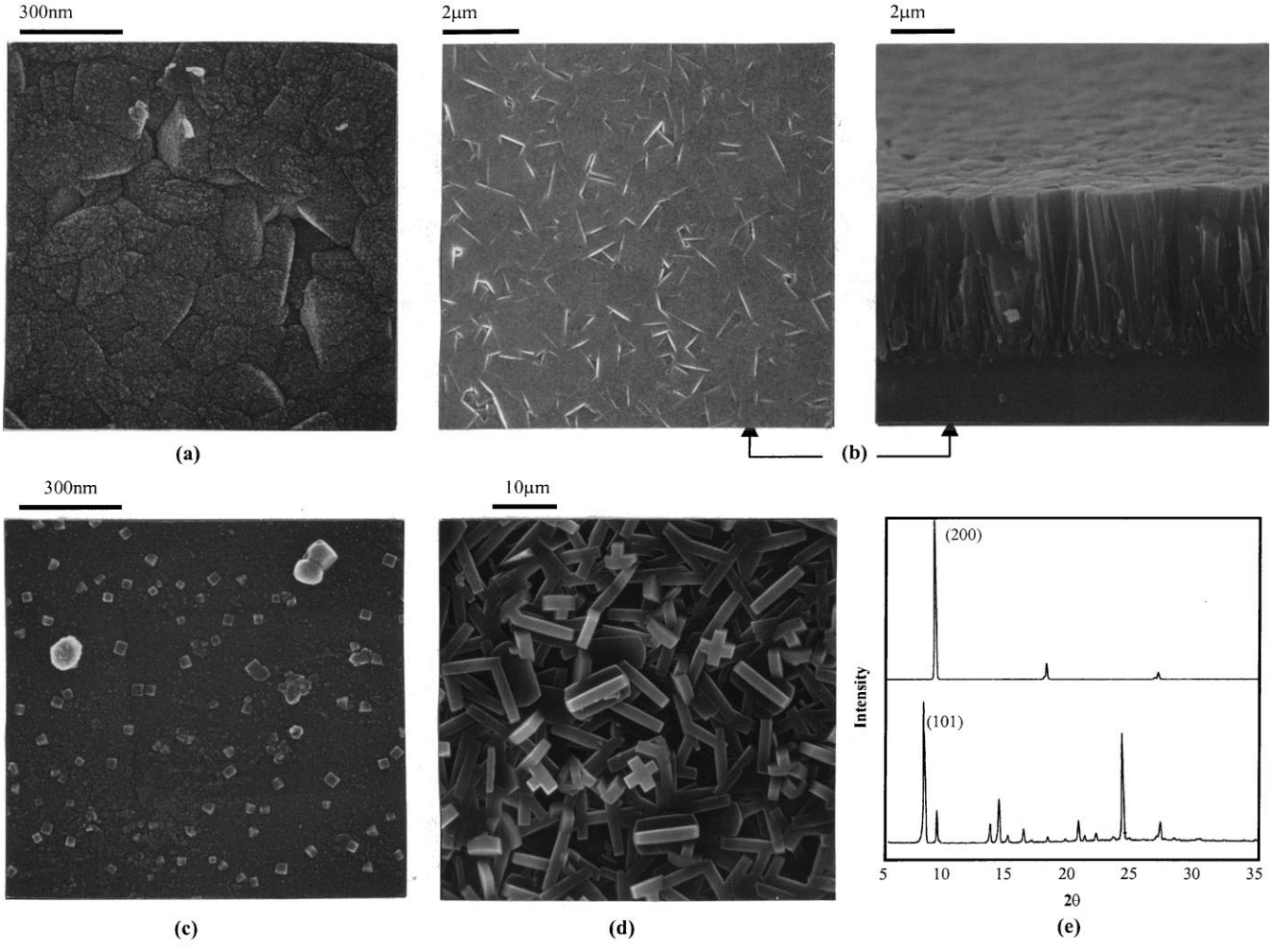

Fig. 2. SEM micrographs of films prepared by secondary growth (a, b), and *in situ* growth, (c, d); after 4 h, (a, c); and 20 h (b, d). Corresponding XRD patterns, (e), for the films obtained by secondary growth (bottom) and *in situ* growth (top). The initial composition of the reaction mixture was 4 SiO_2 : 0.9 TPAOH : 950 H_2O : 16 EtOH and the temperature was 140°C.

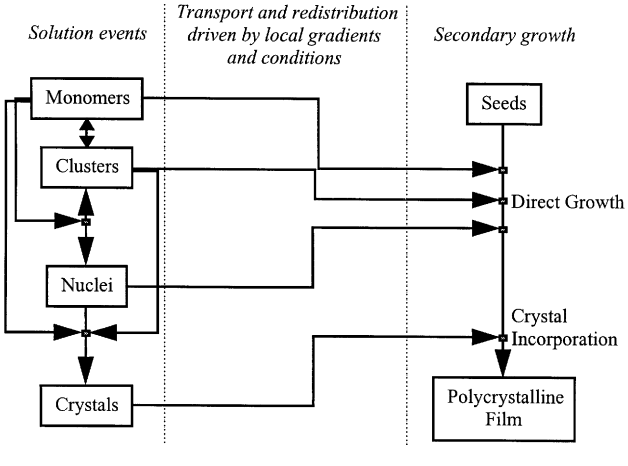

Fig. 3. Events taking place upon hydrothermal treatment and in the presence of precursor seeds.

explanation for the absence of new grain formation during secondary growth, even under conditions which can lead to nucleation and growth in solution. In this respect, the role of the precursor layer is dual. It not only leads to growth without the need for nucleation but also may prohibit or limit the incorporation of newly formed crystals. Based on the above, the final film quality will depend on the quality of the precursor layer. The absence of close-packed precursor seeds throughout the area of the substrate can contribute to the development of defects. Typical defects that are observed by SEM are presented in Fig. 4. As can be seen from this figure, some grains appear to grow larger and to an inclination compared to the rest of the columnar grains that form the dense polycrystalline film. These larger grains extend above the film surface, constituting a hemispherical dome. The formation of these defects is attributed

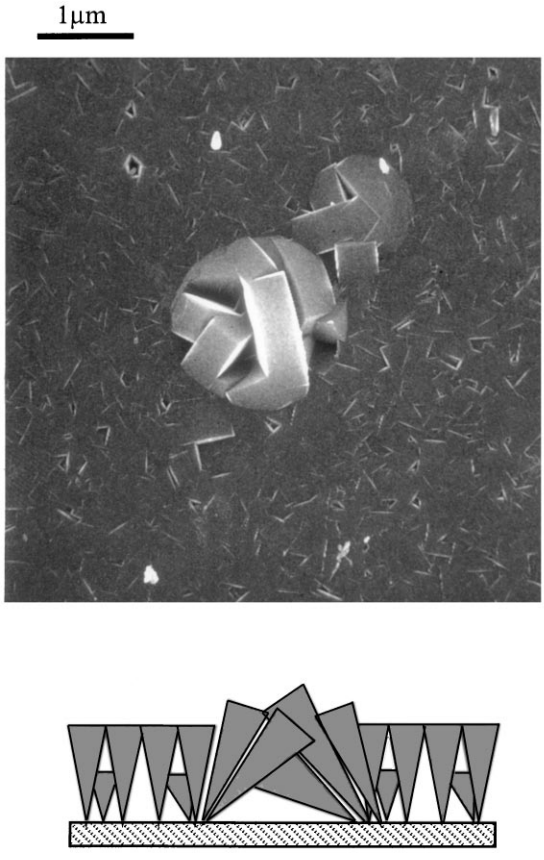

Fig. 4. Typical dome-like defects for films prepared by secondary growth.

to the absence of a close-packed precursor layer underneath the area of the defect, allowing for a less-competitive growth in this neighborhood and resulting in the inclined, less intergrown, and larger grains shown in Fig. 4.

3.2. Manipulation of the film orientation

As mentioned in Section 3.1, the films after secondary growth at 140°C exhibit [$h\,0\,h$]-out-of-plane orientation. This preferred orientation can be altered if secondary growth is carried out at higher temperature (175°C). In Fig. 5a, a SEM cross-section of a film obtained by secondary growth at 175°C is presented. From the corresponding XRD (Fig. 5b) it can be concluded that the film exhibits *c*-out-of-plane orientation. This is further verified by the pole figure line plots (Fig. 5c). The (0 0 2) reflection shows a maximum at 0° tilt angle indicating that the *c*-axis of the grains is perpendicular to the substrate.

The [$h\,0\,h$]-out-of-plane orientation that the films exhibit after secondary growth at 140°C can be enhanced, if the secondary growth is sustained for prolonged times. This can be achieved by replenishing the secondary growth solution periodically. A film obtained with sustained secondary growth at 140°C is presented in Fig. 5d. The corresponding XRD and pole figure (Figs. 5e and f, respectively) show that in this case the *c*-axes of the grains are tilted to an angle of 34° with respect to the normal.

The difference in the grain structure between the films prepared under sustained growth at 140°C and secondary growth at 175°C can be revealed also by SFM topography. In the case of the film obtained upon sustained growth at 140°C, the SFM images (Fig. 6a) show grains of single faces of angular tilt of $10 \pm 5°$ towards the glass substrate plane. In conjunction with the XRD results it can be concluded that they are the (101) faces of the grains, lying nearly perpendicular to the normal. In the case of the film obtained at 175°C, the SFM images of Fig. 6b show faceted grains with two crystal faces. Furthermore, lateral force measurements show enhanced contrast of the two crystal faces in each grain (Fig. 6c). It is important to note that the contrast in Fig. 6c is due to topography and not because of differences in mechanical properties. Hence, the here presented lateral force measurements do not represent dissipative frictional contrast information. This has been confirmed by scanning in reversed direction, which provided the same contrast information. Frictional contrast would be reversed as discussed in detail elsewhere (Overney and Meyer, 1993). Considering these SFM results along with the XRD results of Fig. 5c, it can be concluded that the crystal faces in Figs. 6b and c are the $\{1\,0\,1\}$ faces of coffin-shaped grains lying at an angle with the normal. Besides temperature variation, the film microstructure can also be manipulated by varying the composition of the secondary growth mixture and the precursor seed morphology, as will be described elsewhere.

3.3. MFI membranes and permeation results

3.3.1. Membrane morphology

Fig. 7a shows SEM top views of the α-Al_2O_3 porous support (left) and a smooth layer of equiaxed silicalite-1 seeds with diameter $\sim$100 nm covering the support after dip-coating (right). Secondary growth of the seed layers was carried out as described in Section 2.1. Fig. 7b shows a SEM cross-section and the XRD pattern of the surface of the membrane obtained after a single regrowth of 24 h at 175°C with M = Na, while Fig. 7c shows the corresponding results for a membrane grown by two consecutive regrowths under identical conditions. The XRD pattern of Fig. 7b indicates the onset of *c*-out-of-plane orientation. The XRD pattern of Fig. 7c shows a strong (0 0 2) peak and therefore a pronounced *c*-orientation of the membrane. After one secondary growth for 24 h at 175°C the resulting *c*-oriented crystals have a length of $\sim$12–15 μm along the *c*-direction. The thickness doubles

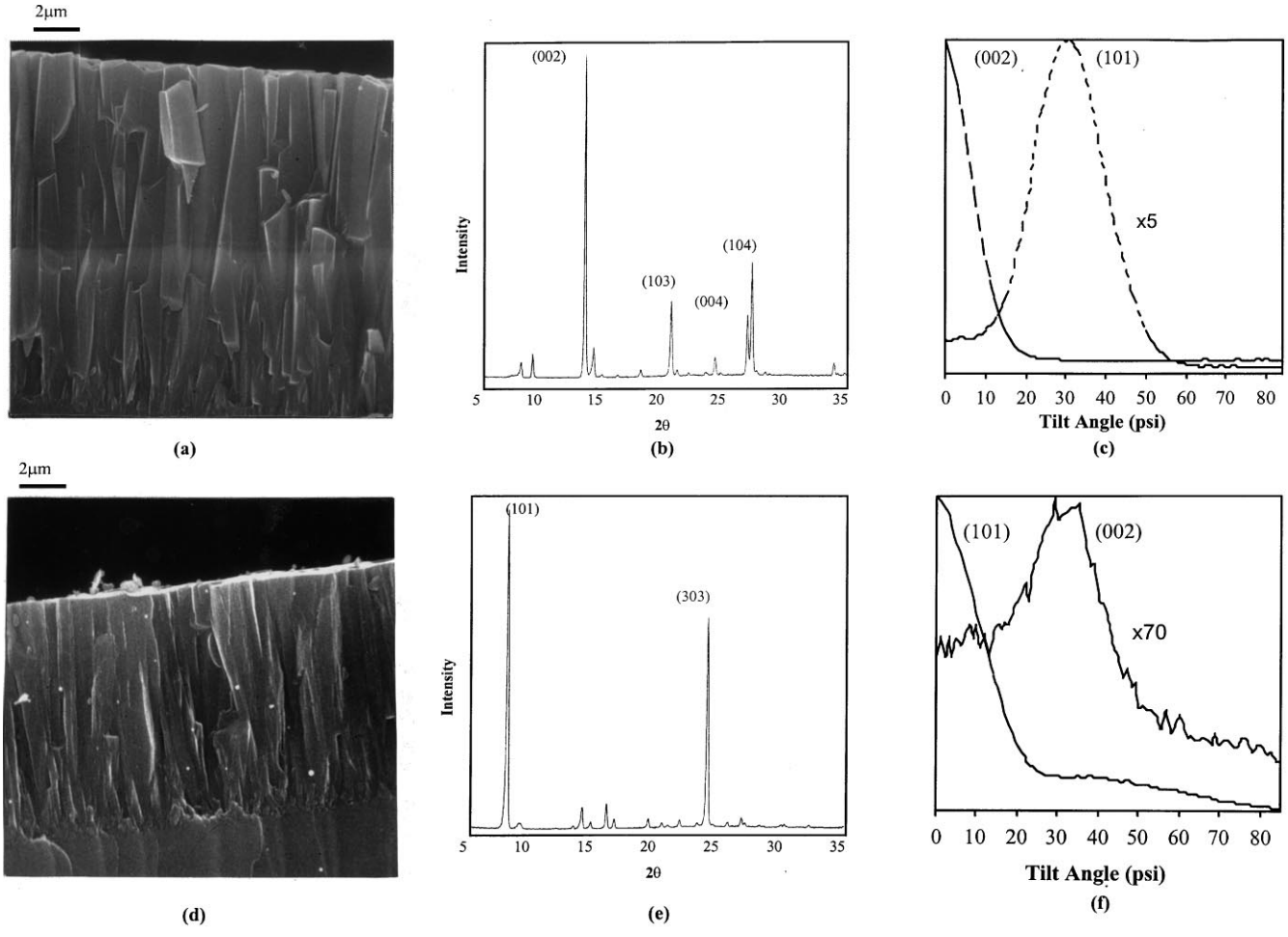

Fig. 5. SEM cross-sections, (a), (d); XRD patterns, (b), (e); and (0 0 2) and (1 0 1) pole figure line plots, (c), (f); for films obtained by secondary growth at 175°C (a)–(c) and sustained secondary growth at 140°C (d)–(f).

after subjecting the membranes to an additional growth at similar conditions. The SEM cross-sections shown in Fig. 7 indicate that the secondary growth of silicalite-1 seeds results in the formation of continuous films of tightly packed MFI crystals that, at least within the SEM resolution, possess a high degree of intergrowth necessary for membrane applications. These zeolite films however, are not free of defects that may form undesirable non-selective pathways in parallel with the zeolitic pores. Defects occasionally observed on the film surface are cracks or holes between the zeolite crystals, crystals incorporated in the zeolite film by precipitation from solution, or dome-like defects formed in areas where continuity of the seed layers was interrupted. Examples of such defects are shown in Fig. 8. Grain boundaries between adjacently grown zeolite crystals are also considered to be another source of non-selective pathways that may transverse the entire zeolite film thickness. These grain boundaries are however inherent to the membrane structure and their concentration and size are more likely affected by the secondary growth conditions rather than by defects formed in the precursor seed layers.

3.3.2. Membrane permeation

Table 1 summarizes binary permeation data of butane isomers at 22°C for several membranes prepared under the conditions given in Section 2.1. Membranes M1-M6 were synthesized with M = Na, while M7 and M8 were prepared with M = K. The binary n-C_4 : i-C_4 ratios are typically in the range of 28–62, while the n-C_4 permeation flux is in the range $1.5–5.5 \times 10^{-3}$ mol m^{-2} s^{-1} and apparently decreases with increasing membrane thickness. Fig. 9a gives the temperature dependence of the flux of butane isomers from a 50/50 binary feed for membrane M7. Temperature cycling was also carried out on membrane M7 to determine the stability of the membrane permeation properties. The n-C_4 and i-C_4 fluxes showed

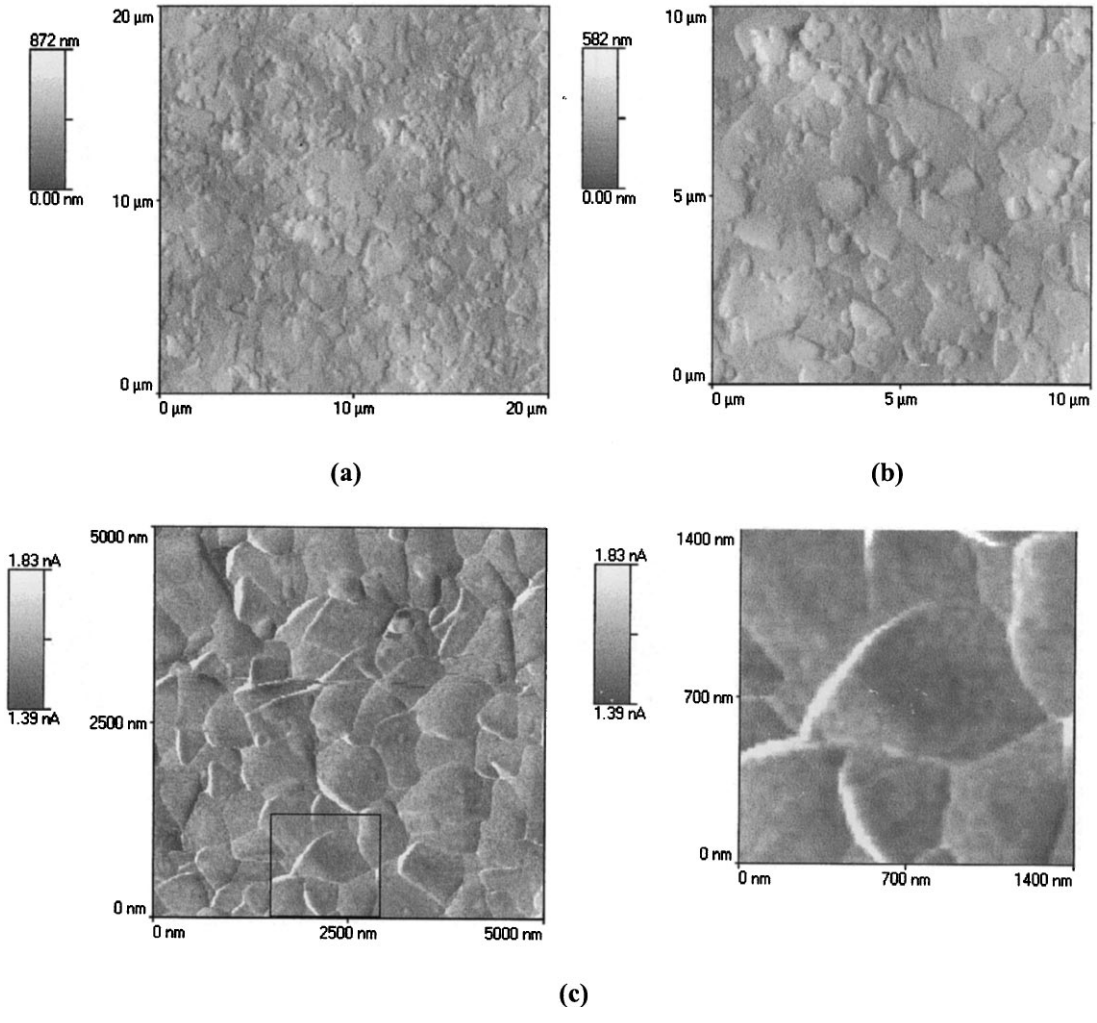

Fig. 6. SFM topography images of films obtained by sustained secondary growth at 140°C after 50 h, (a); and of films obtained by secondary growth at 175°C after 5 h, (b). SFM lateral force forward image, (c), of the film shown in (b).

no significant variation between two heating cycles (performed over a period of 3 days), indicating that the permeation of butanes has no modifying effect on the membrane. The numbers above the n-C_4 data points indicate the n-C_4 : i-C_4 flux ratio during the first heating cycle (△, ▲), while the numbers below indicate the flux ratio during the second heating cycle (▽, ▼). The flux of n-C_4 shows a weak maximum at 140–150°C while the flux of i-C_4 increases monotonically with temperature, so that the n-C_4 : i-C_4 ratio remains high up to about 180°C but drops to about 15 at higher temperatures. Fig. 9b shows the effect of feed composition on the flux of butane isomers at 22°C for membrane M8. The butane partial pressure in the feed was adjusted to the desired level by diluting a 50/50 butane mixture with necessary amount of He. The data indicate that saturation of the MFI-type membranes at 22°C is effected at about 0.2 atm partial pressure of butane isomers in the feed. Also included in Table 1 are N_2 and SF_6 single-component permeation data at 22°C for the support and membrane M3, which was prepared by 2 sequential growths. The MFI layer results in a maximum of 3–5 times permeance reduction for N_2 relative to the porous support and improvement of the N_2 : SF_6 ratio from 2 (Knudsen selectivity) to 7–10. For the same membranes before calcination for template removal, the N_2 flux was $\sim 5 \times 10^{-5}$ mol m^{-2} s^{-1}, e.g. 3 orders of magnitude lower than the flux through the support.

The permeation data above suggest that gas transport through the MFI-type membranes occurs in parallel through the MFI pores and the film defects which most likely consist of the intercrystalline grain boundaries between adjacent crystals. The flux through the defects is estimated to be in the range 10^{-5} mol m^{-2} s^{-1} based on n-C_4H_{10} and i-C_4H_{10} permeation flux through uncalcined membranes. Since zeolitic pores are occupied

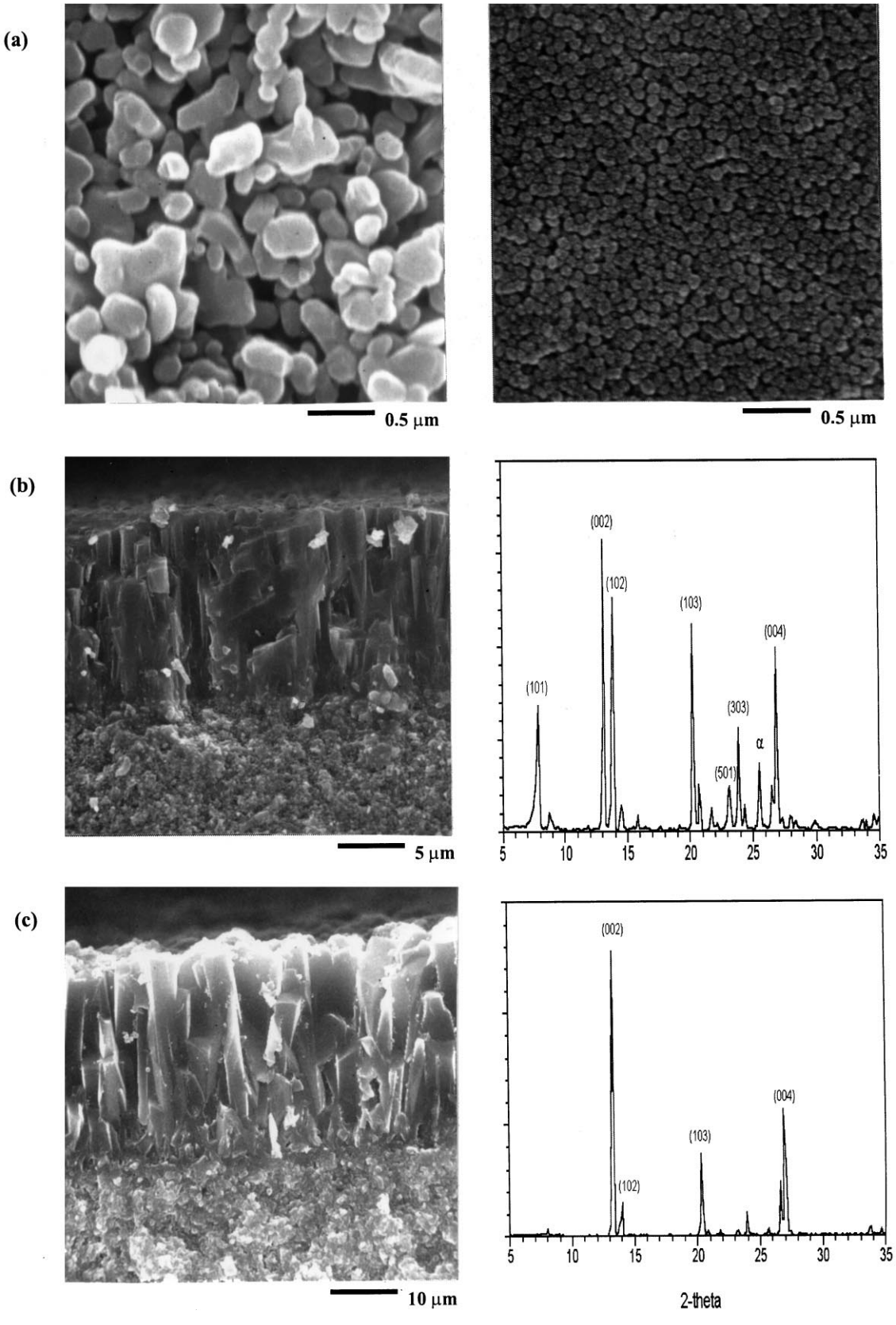

Fig. 7. SEM images of: (a) α-Al_2O_3 support (left) and silicalite seed layer formed by dip coating; (b) MFI membrane formed after a single regrowth, with XRD pattern; and (c) after two consecutive regrowths, with XRD pattern.

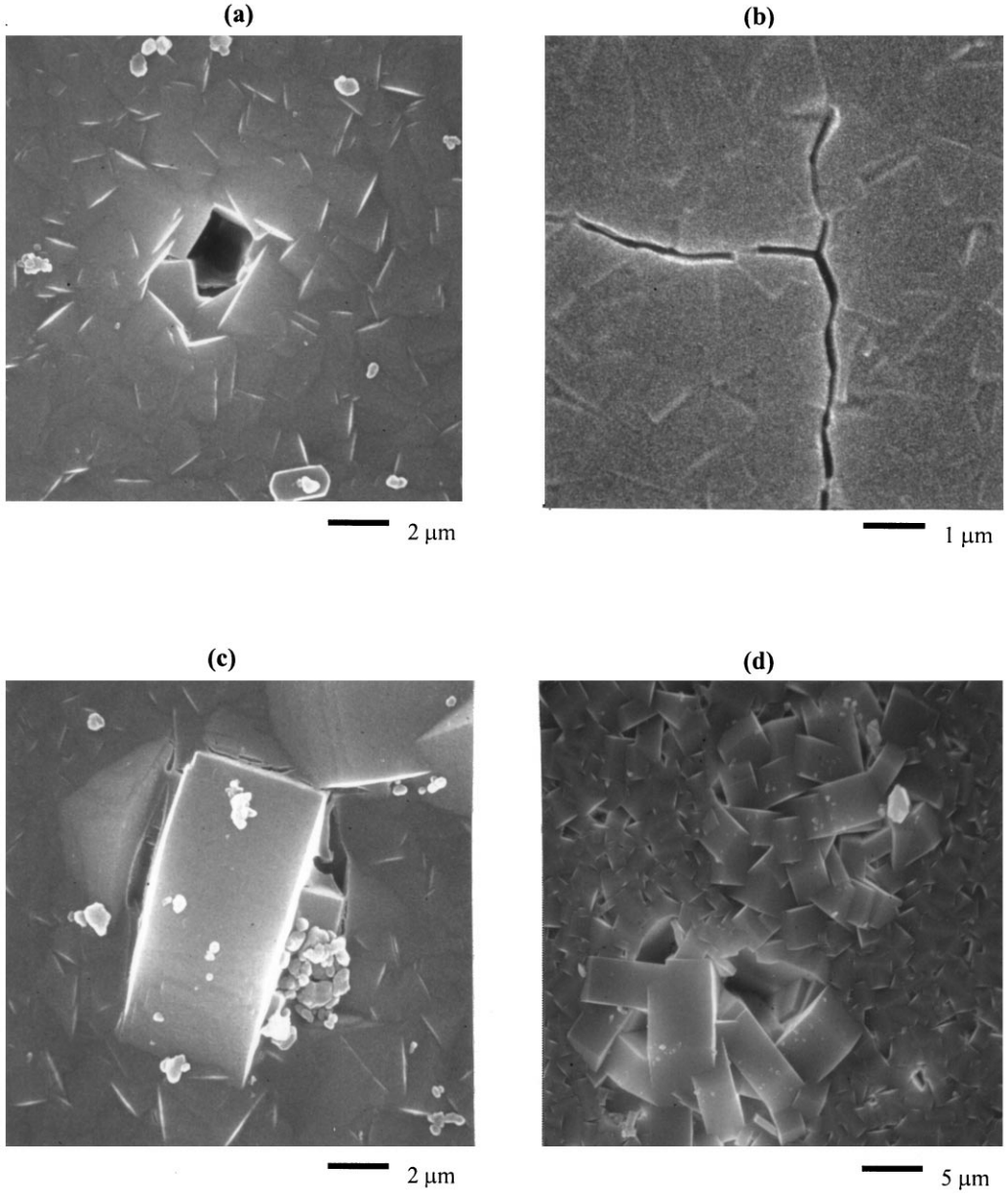

Fig. 8. SEM views of defects found on the surface of MFI-type membranes: (a) hole; (b) crack between zeolite crystals; (c) crystal incorporated from solution during secondary growth; (d) dome-like defect.

by the template before calcination, the detected flux was attributed to flux through the defects. The flux through the zeolitic pores is in the range 10^{-2} mol m^{-2} s^{-1} for small molecules such as N_2 and in the range 10^{-3} mol m^{-2} s^{-1} for larger molecules such as n-C_4H_{10} and SF_6. For i-C_4H_{10} the permeation flux at 22°C is in the range 10^{-5} mol m^{-2} s^{-1} but increases more than 20 times at 200°C. This indicates that diffusion of i-C_4H_{10} through the zeolitic pores at ambient is rather small, comparable or smaller to that through the defects, but increases with temperature.

Table 2 summarizes results of various workers on permeation of butane isomers through MFI-type membranes prepared by in-situ crystallization. In all cases, a high ideal or mixture selectivity for n-C_4H_{10} over i-C_4H_{10} is observed (Geus et al., 1993; Yan et al., 1995; Vroon et al., 1996; Kusakabe et al., 1996). Coronas et al. (1997) reported i-C_4H_{10} : n-C_4H_{10} ideal selectivities > 1 at ambient temperatures but their membranes always selectively permeated the linear isomer in 50/50 mixtures of the two components. In addition, most workers report n-C_4H_{10} permeation flux in the 10^{-3} mol m^{-2} s^{-1} range

Table 1
Permeation flux of butane isomers through various MFI-type membrane samples at 22°C

Code	No. of regrowths	Permeation flux ($mol\,m^{-2}\,s^{-1}$)		Flux ratio
		n-C_4H_{10} (N_2)[a]	i-C_4H_{10} (SF_6)[a]	n-C_4 : i-C_4 (N_2:SF_6)
Support[b]	—	5.04×10^{-2}	5.04×10^{-2}	1.0
		(6.94×10^{-2})	(3.37×10^{-2})	(2.06)
M1	1	4.28×10^{-3}	1.50×10^{-4}	28.5
M2	1	5.47×10^{-3}	1.13×10^{-4}	48.3
M3	2	1.59×10^{-3}	4.28×10^{-5}	37.1
		(1.61×10^{-2})	(1.61×10^{-3})	(10.0)
M4	2	1.78×10^{-3}	2.90×10^{-5}	61.4
M5	2	2.05×10^{-3}	3.49×10^{-5}	58.7
M6	2	1.74×10^{-3}	3.71×10^{-5}	46.9
M7	2	2.96×10^{-3}	4.79×10^{-5}	61.8
M8	2	1.80×10^{-3}	4.67×10^{-5}	38.6

[a]N_2, SF_6 single-component fluxes and selectivity included for support and membrane M3.
[b]Butane flux determined from single-component permeation measurements.

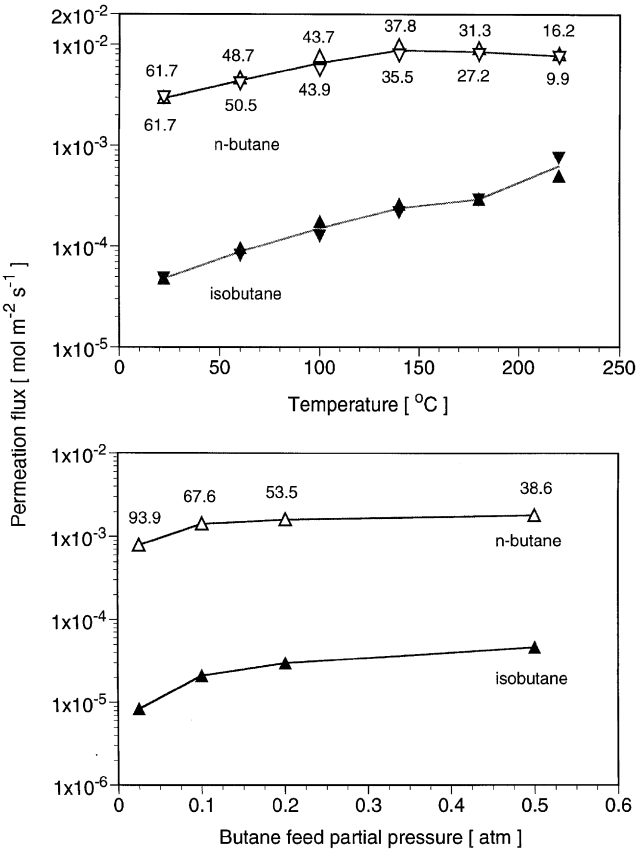

Fig. 9. Permeation properties of membranes M7 and M8: (a) temperature dependence and effect of temperature cycling (M7); (b) dependence on feed butane partial pressure (M8).

which is also consistent with the data obtained in this study. The temperature dependence of the flux of butane isomers through the membranes reported here is consistent with that reported by Vroon et al. (1996) and Burggraaf et al. (1998), since their flux of n-C_4H_{10} exhibited a weak maximum at 100–140°C while the flux of i-C_4H_{10} increased monotonically in the range 22–200°C. Similar agreement is observed between the feed partial pressure dependence of the flux of n-C_4H_{10} with the corresponding data of Vroon et al. (1996) and Yan et al. (1997). Coronas et al. (1997, 1998) reported a high $N_2:SF_6$ single gas ratio (100–200) and concluded that their membranes exhibited molecular sieving properties since they practically reject SF_6 (kinetic diameter $\sim$6 Å). For the membranes reported here, the $N_2:SF_6$ ratio was about 10 although the n-C_4:i-C_4 ratio was significant. Similar results are reported by Burggraaf et al. (1998), since their membranes exhibited permeances in the order n-$C_4 > SF_6 > i$-C_4 which is consistent with that of the membranes reported here. The membranes reported in the present study also exhibit permselectivity for xylene isomers (Xomeritakis and Tsapatsis, 1999).

4. Conclusions

Secondary growth of precursor seeds can be used to prepare selective MFI membranes. The presence of the precursor film drastically alters the mechanism of film formation from that of *in situ* growth. The microstructure of the membranes can be manipulated by varying the secondary growth conditions. The high n-C_4 and i-C_4 fluxes, and the high n-C_4 : i-C_4 binary mixture selectivities indicate that membranes with c-out-of-plane preferred orientation prepared by secondary growth can exhibit transport properties for these gases resulting in similar performance with the most selective randomly

Table 2
Permeation of butane isomers through highly selective MFI-type membranes prepared by *in situ* crystallization

Reference	Permeation temperature[a] (°C)	Permeation flux (mol m^{-2} s^{-1})		Flux ratio n-C_4 : i-C_4
		n-C_4H_{10}	i-C_4H_{10}	
Kusakabe et al. (1996)	100	3.0×10^{-3}	7.0×10^{-5}	43
Yan et al. (1997)	185	2.7×10^{-3}	6.0×10^{-5}	45
Coronas et al. (1998)	100	5.4×10^{-3}	1.0×10^{-4}	54
Vroon et al. (1998)	25	3.8×10^{-3}	2.9×10^{-5}	131

[a] Temperature at which the highest selectivity was achieved.

oriented MFI membranes prepared by *in situ* growth reported in the literature.

Acknowledgements

Support for this work was provided by NSF [CTS-9624613 (CAREER) and CTS-9512485 (ARI)]. M.T. is grateful to the David and Lucile Packard Foundation for a Fellowship in Science and Engineering and the Dreyfus Foundation for a Camille and Henry Dreyfus Teacher-Scholar Award.

References

Bein, T. (1996). Synthesis and applications of molecular sieve layers and membranes. *Chem. Mater.*, *8*, 1636–1653.

Boudreau, L.C., & Tsapatsis, M. (1997). A highly oriented thin film of zeolite A. *Chem. Mater.*, *9*, 1705–1709.

Boudreau, L.C., Kuck, J.A., & Tsapatsis, M. (1998). Deposition of oriented zeolite A films: *in situ* and secondary growth. *J. Membr. Sci.* *152*, 41.

Brinker, J.C. (1998). Oriented inorganic films. *Curr. Opin. Colloid Interface Sci.*, *3*, 166–173.

Burggraaf, A.J., Vroon, Z.A.E.P., Keizer, K., & Verweij, H. (1998). Permeation of single gases in thin zeolite MFI membranes. *J. Membr. Sci.*, *144*, 77.

Burkett, S.L., & Davis, M.E. (1995a). Mechanisms of structure direction in the synthesis of pure–silica zeolites. 1. Synthesis of TPA/Si-ZSM-5. *Chem. Mater.*, *7*, 920–928.

Burkett, S.L., & Davis, M.E. (1995b). Mechanisms of structure direction in the synthesis of pure–silica zeolites. 2. Hydrophobic Hydration and structural specificity. *Chem. Mater.*, *7*, 1453–1463.

Coronas, J., Falconer, J.L., & Noble, R.D. (1997). Characterization and permeation properties of ZSM-5 tubular membranes. *A.I.Ch.E. J.*, *43*, 1797–1812.

Coronas, J., Noble, R.D., & Falconer, J.L. (1998). Separation of C_4 and C_8 isomers in ZSM-5 Tubular Membranes. *Ind. Engng Chem. Res.*, *37*, 166.

Dokter, W.H., Van Garderen, H.F., Beelen, T.P.M., Van Santen, R.A., & Bras, W. (1995). Homogeneous versus heterogeneous zeolite nucleation. *Angew. Chem. Int. Ed. Engl.*, *34*, 73–75.

Geus, E.R., Bekkum, H., Bakker, W.J.W., & Moulijn, J.A. (1993). High-temperature stainless steel supported zeolite (MFI) membranes: Preparation, module construction, and permeation experiments. *Microporous Mater.*, *1*, 131–147.

Gouzinis, A., & Tsapatsis, M. (1998). On the preferred orientation and microstructural manipulation of molecular sieve films prepared by secondary growth. *Chem. Mater.* *10*, 2497.

Koegler, J.H., Bekkum, H., & Jansen, J.C. (1997). Growth model of oriented crystals of zeolite Si-ZSM-5. *Zeolites*, *19*, 262–269.

Kusakabe, K., Yoneshige, S., Murata, A., & Morooka, S. (1996). Morphology and gas permeance of ZSM-5-type zeolite membrane formed on a porous α-alumina support tube. *J. Memb. Sci.*, *116*, 39.

Lai, W.F., Deckman, H.W., McHenry, J.A., & Verduijn, J.P. (1996). Zeolite layers with controlled crystal width and preferred orientation grown on a growth enhancing layer. *International Patent Application* WO96/01687.

Lovallo, M.C., & Tsapatsis, M. (1996). Preferentially oriented submicron silicalite membranes. *A.I.Ch.E. J.*, *42*, 3020–3029.

Lovallo, M.C., Tsapatsis, M., & Okubo, T. (1996). Preparation of an asymmetric zeolite L film. *Chem. Mater.*, *8*, 1579–1583.

Lovallo, M.C., Gouzinis, A., & Tsapatsis, M. (1998). Synthesis and characterization of oriented MFI membranes prepared by secondary growth. *A.I.Ch.E. J.*, *44*, 1903–1913.

Overney, R.M., & Meyer, E. (1993). Tribological investigations using friction force microscopy. *Mater. Res. Soc.*, *18*, 26–34.

Vroon, Z.A.E.P., Keizer, K., Gilde, M.J., Verweij, H., & Burggraaf, A.J. (1995). Transport properties of alkanes through ceramic thin MFI membranes. *J. Memb. Sci.*, *113*, 293–300.

Vroon, Z.A.E.P., Keizer, K., Gilde, M.J., Verweij, H., & Burggraaf, A.J. (1996). Transport properties of alkanes through ceramic thin zeolite MFI membranes. *J. Memb. Sci.*, *113*, 293.

Vroon, Z.A.E.P., Keizer, K., Gilde, M.J., & Verweij, H. (1998). Preparation and characterization of thin zeolite MFI membranes on porous supports. *J. Memb. Sci.*, *144*, 65.

Xomeritakis, G., & Tsapatsis, M. (1999). *Chem. Mater.* (in press).

Yan, Y., Tsapatsis, M., Davis, M.E., & Gavalas, G.R. (1995). Zeolite ZSM-5 membranes on porous α-Al_2O_3. *J. Chem. Soc. Chem. Commun.*, 227–228.

Yan, Y., Davis, M.E., & Gavalas, G.R. (1997). Preparation of highly selective zeolite ZSM-5 membranes by a post-synthetic coking treatment. *J. Memb. Sci.*, *123*, 95.